A Simple Geometrically Exact Finite Element for Thin Shells

Matheus L. Sanchez[1], Paulo M. Pimenta[1], Adnan Ibrahimbegovic[2]

[1] *Polytechnic School at University of São Paulo Av. Prof. Almeida Prado, travessa 2, 83, São Paulo, SP 05424-970, Brazil matheusanchez@gmail.com, ppimenta@usp.br*
[2] *Université de Technologie de Compiègne, Compiègne (UTC) Centre de Recherches Royallieu, Université de Technologie de Compiègne, Compiègne 60203, France adnan.ibrahimbegovic@utc.fr*

Abstract. In this Article, we present a shell finite element, with 6 nodes, and a special non-conforming rotational field constructed from an incremental scalar rotation variable and displacement field. This approach eliminates the need for any numerical techniques such as penalties or Lagrange multipliers to address C1 continuity, a kinematic requirement for Kirchhoff-Love shell theory. The quadratic displacement field of the mid-plane is represented by the standard degree-of-freedom at the element's 6 nodes. The element has been tested under very different simulations scenarios ans has proved to be a reliable element for simulation of thin shells even for large displacements, rotations and strains.

Keywords: Finite element method, Kirchhoff-Love Shell, nonlinear, Geometrically Exact.

1 Introduction

Shell Finite Elements (FEM) hold significant research importance even in present days due to their widespread applications in structural engineering, such as slabs, domes, metal sheets, and other thin structures. However, when dealing with simulations of extremely thin structures, there can be numerical challenges with existing finite element software. These challenges are generally related to the unrealistic stiffness of the shell (or thin 3D domain) at the FEM routine level, leading to untrustworthy results.

To address this issue and to seek a more straightforward, simple and reliable approach, the authors have developed the current model (See [1]). This work builds upon the findings of previous studies conducted by the group (refer to [2], [3], [4] and [5]. The main focus of this research is to introduce a novel technique for enforcing C1 displacement continuity uniquely based on shell kinematics and shell usual degrees of freedom, with out the use of known numerical tools, such as penalty, Lagrange methods or special spacial shape functions.

The exact shell finite element developed here is suitable for simulation of very thin structures with both large displacements, rotations and strains. It have been recently published in [1], and is presented here to summarize recent advances. The shell simulations, reveals trusty and reliable results for very different numerical examples, demonstrating the importance of this recent development and promising advancements in the field of structural engineering.

2 Shell Model

2.1 Shell Kinematics

The kinematics of this shell element is established based on the following conceptual framework. The critical kinematic variables are presented in Figure 1. The shell's kinematics is based in two configurations: the initial configuration, termed the "reference configuration," which remains constant over time (midle surface of the shell referred as $\Omega^r \subset \mathbb{R}^2$ with its boundary as $\Gamma^r = \partial\Omega^r$), and the subsequent configuration (current configuration) depicting the shell's position through various time steps within the simulation.

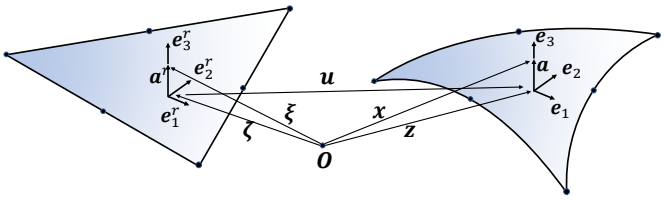

Figure 1. Shell kinematics.

The shell middle surface of the current configuration is parameterized as $\Omega \subset \mathbb{R}^3$ with its boundary as $\Gamma = \partial\Omega$. Both configurations, the reference and the current, incorporate thickness and volume parameters (V^r and V, respectively).

For simplicity, it is assumed that the midle surfaces Ω^r and Ω consistently lie within the middle thickness of the shell, with the shell's thickness being described by the parameter range $H^r = [-h^r/2, +h^r/2]$ (where shell thickness $= h^r$).

The reference configuration is defined together with an orthonormal right-handed coordinate system (RCCS): $\boldsymbol{e}_i^r$ situated on Ω^r. The third vector of this RCCS is orthogonal to the shell's central surface. An origin O serves as a significant fixed point for all configurations and is employed for kinematic descriptions. Any point "P" on the shell in the current configuration corresponds to a point in the reference configuration's $\boldsymbol{e}_i^r$ system. The position of an arbitrary point "P^r" in the RCCS is articulated by the equation:

$$\boldsymbol{\xi} = \boldsymbol{\zeta} + \boldsymbol{a}^r \ , \tag{1}$$

where $\boldsymbol{\zeta} = \xi_\alpha \boldsymbol{e}_\alpha^r$, $\xi_\alpha \in \Omega^r$ is the vector connecting the fixed point O to the projection of P^r onto the reference plane Ω^r, and $\boldsymbol{a}^r = \xi_3 \boldsymbol{e}_3^r$, $\xi_3 \in H^r$, represents a normal vector to the reference plane (director vector). It's worth noting that ξ_1, ξ_2, ξ_3 establishes a three-dimensional Cartesian framework.

The corresponding point P in the current configuration is parameterized as follows:

$$\boldsymbol{x} = \boldsymbol{z} + \boldsymbol{a} \ , \tag{2}$$

where $\boldsymbol{x} = \hat{\boldsymbol{x}}(\boldsymbol{\xi})$ denotes the vector field that defines the shell's motion and, consequently, the position of P in relation to the fixed origin O, $\boldsymbol{z}$ signifies its position within the middle-surface, and $\boldsymbol{a}$ represents its director. This leads to the relationship:

$$\boldsymbol{z} = \boldsymbol{\zeta} + \boldsymbol{u} \ , \tag{3}$$

where $\boldsymbol{u}$ signifies the displacement of the shell's central plane.

A pivotal element of the shell's kinematics is the introduction of the rotation tensor $\boldsymbol{Q}$, which represents the rotation of the coordinate basis from the reference configuration ($\boldsymbol{e}_i^r$) to the current configuration ($\boldsymbol{e}_i$), specifically utilized in this formulation for the rotation of the director vector. This is expressed by the equations:

$$\boldsymbol{Q} = \boldsymbol{e}_i \otimes \boldsymbol{e}_i^r \quad , \ i \in 1,2,3 \quad \text{and} \quad \boldsymbol{a} = \boldsymbol{Q}\boldsymbol{a}^r \quad . \tag{4}$$

The detailed parametrization of the tensor $\boldsymbol{Q}$ is elaborated upon in Section 2.2.

The calculation of the deformation gradient ($\boldsymbol{F}$) is carried out using the following expression:

$$\boldsymbol{F} = \frac{\partial \boldsymbol{x}}{\partial \boldsymbol{\xi}} = \frac{\partial(\boldsymbol{z} + \boldsymbol{Q}\boldsymbol{a}^r)}{\partial \xi_\alpha} \otimes \boldsymbol{e}_\alpha^r + \frac{\partial\left(\boldsymbol{z} + \boldsymbol{Q}\boldsymbol{a}^r\right)}{\partial \xi_3} \otimes \boldsymbol{e}_3^r, \tag{5}$$

which can be simplified as

$$\boldsymbol{F} = \boldsymbol{f}_\alpha \otimes \boldsymbol{e}_\alpha^r + \boldsymbol{f}_3 \otimes \boldsymbol{e}_3^r \quad \text{where,} \quad \boldsymbol{f}_\alpha = \boldsymbol{z}_{,\alpha} + \boldsymbol{Q}_{,\alpha}\boldsymbol{a}^r \quad \text{and} \quad \boldsymbol{f}_3 = \boldsymbol{Q}\boldsymbol{e}_3^r = \boldsymbol{e}_3 \ . \tag{6}$$

Here, the first and second derivatives of $\boldsymbol{z}$ are computed as (using Equation 3)

$$\boldsymbol{z},\alpha = \boldsymbol{e}\alpha^r + \boldsymbol{u},\alpha \quad \text{and} \quad \boldsymbol{z},\alpha\beta = \boldsymbol{u},\alpha\beta \quad \text{with } (\bullet),\alpha = \frac{\partial(\bullet)}{\partial \xi_\alpha} \quad . \tag{7}$$

Equation 6 can be rephrased using curvature vector and tensors as

$$\boldsymbol{f}\alpha = \boldsymbol{z},\alpha + \boldsymbol{\kappa}_\alpha \times \boldsymbol{a} \quad \text{with} \quad \boldsymbol{K}_\alpha = \boldsymbol{Q}_{,\alpha}\boldsymbol{Q}^T \quad \text{and} \quad \boldsymbol{\kappa}\alpha = \text{axial}\left(\boldsymbol{K}\alpha\right) \quad . \tag{8}$$

Next, we introduce the back-rotated deformation gradient $\boldsymbol{F}^r$ as follows:

$$\boldsymbol{F}^r = \boldsymbol{Q}^T \boldsymbol{F} = \boldsymbol{Q}^T (\boldsymbol{f}_\alpha \otimes \boldsymbol{e}_\alpha^r + \boldsymbol{f}_3 \otimes \boldsymbol{e}_3^r) \quad , \tag{9}$$

$$\boldsymbol{F}^r = \boldsymbol{Q}^T (\boldsymbol{z}_{,\alpha} + \boldsymbol{\kappa}_\alpha \times \boldsymbol{a}) \otimes \boldsymbol{e}_\alpha^r + \boldsymbol{e}_3^r \otimes \boldsymbol{e}_3^r \quad \text{and} \quad \boldsymbol{F}^r = I + \boldsymbol{\gamma}_\alpha^r \otimes \boldsymbol{e}_\alpha^r \quad . \tag{10}$$

In Equation 10, we introduce the concept of back-rotated strains and generalized back-rotated cross-section strains:

$$\boldsymbol{\gamma}_\alpha^r = \boldsymbol{\eta}_\alpha^r + \boldsymbol{\kappa}_\alpha^r \times \boldsymbol{a}^r \quad , \quad \text{with} \quad \boldsymbol{\eta}_\alpha^r = \boldsymbol{Q}^T \boldsymbol{z}_{,\alpha} - \boldsymbol{e}_\alpha^r \quad \text{and} \quad \boldsymbol{\kappa}_\alpha^r = \text{axial}\left(\boldsymbol{Q}^T \boldsymbol{Q}, \alpha\right) \quad , \tag{11}$$

where $\boldsymbol{\eta}_\alpha^r$ represents the membrane deformation strains and $\boldsymbol{\kappa}_\alpha^r$ represents the bending strains.

2.2 Rotations

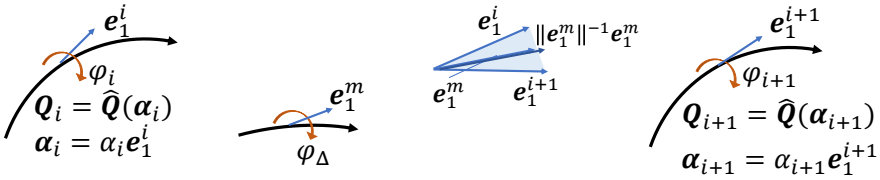

Figure 2. Rotation about a moving axis. Here, φ_Δ is a scalar quantity that may be understood as the incremental rotation applied to the body over the average axis $\boldsymbol{e}^m$. In this article, we use the element side as the moving axis of this incremental rotation.

We can express the absolute rotation θ around an axis $\boldsymbol{e}$ using the rotation vector $\boldsymbol{\theta} = \theta \boldsymbol{e}$. However, we parameterize the rotation tensor using the Rodrigues rotation vector $\boldsymbol{\alpha} = \frac{\tan(\theta/2)}{\theta/2}\boldsymbol{\theta}$. Unfortunately, this parameterization confines the rotation within the range of $-\pi < \theta < +\pi$, but this limitation is overcome through an incremental procedure, as elaborated in the next subsection.

In this context, we can define the absolute rotation tensor (refer to Eq. 4 and Ref. [6]) as

$$\boldsymbol{Q} = \boldsymbol{I} + h(\alpha)\left(\boldsymbol{A} + \frac{1}{2}\boldsymbol{A}^2\right) \quad \text{where } h(\alpha) = \frac{4}{4+\alpha^2} \quad , \quad \alpha = \|\boldsymbol{\alpha}\| \quad \text{and} \quad \boldsymbol{A} = \text{Skew}(\boldsymbol{\alpha}) \tag{12}$$

The equations presented previously represent the absolute rotational quantities. One significant advantage of the Rodrigues rotation parameters is the simplicity of incremental description. According to [7], [8], and [9], the incremental rotation description for consecutive simulation steps (i and $i+1$) can be expressed as

$$\boldsymbol{Q}_{i+1} = \boldsymbol{Q}_\Delta \boldsymbol{Q}_i \quad \text{where} \quad \boldsymbol{Q}_{i+1} = \hat{\boldsymbol{Q}}\left(\boldsymbol{\alpha}_{i+1}\right) \quad , \quad \boldsymbol{Q}_\Delta = \hat{\boldsymbol{Q}}(\boldsymbol{\alpha}_\Delta) \quad \text{and} \quad \boldsymbol{Q}_i = \hat{\boldsymbol{Q}}\left(\boldsymbol{\alpha}_i\right) \quad . \tag{13}$$

As $\boldsymbol{Q}$ operates on the director, we can also define that $\boldsymbol{e}_3^{i+1} = \boldsymbol{Q}_\Delta \boldsymbol{e}_3^i$ to update the rotational scheme in our shell formulation. The incremental Rodrigues rotation parameters offer a significant advantage in that we can implement a straightforward update scheme for the absolute rotation vector ($\boldsymbol{\alpha}$) based on the values from previous steps, without needing to construct the rotation tensor (see [10] and [8]). Thus,

$$\boldsymbol{\alpha}_{i+1} = \frac{4}{4 - \boldsymbol{\alpha}_i \cdot \boldsymbol{\alpha}_\Delta} \cdot \left(\boldsymbol{\alpha}_i + \boldsymbol{\alpha}_\Delta - \frac{1}{2}\boldsymbol{\alpha}_i \times \boldsymbol{\alpha}_\Delta\right) \quad , \tag{14}$$

where $\boldsymbol{\alpha}_{i+1}$ represents the consecutive step from $\boldsymbol{\alpha}_i$.

Here, we also employ a significant relation, initially introduced in [11] and [12], where the rotation vector $\boldsymbol{\alpha}_\Delta$ can be expressed as a rotation about a moving axis, utilizing a scalar parameter φ_Δ. This approach was also adopted in [3]. Geometrically, the scalar φ_Δ can be interpreted as a degree of freedom for rotation about a moving axis. This interpretation was applied to rod rotations in earlier work; here, we extend it to shell-director rotations as in [2].

Figure 2 provides a schematic representation of the rotation scheme employed in our formulation. In the left and right regions of the image, two consecutive simulation steps are depicted. The vector $\boldsymbol{e}_1$ undergoes rotation during these steps, transitioning from $\boldsymbol{e}_1^i$ to $\boldsymbol{e}_1^{i+1}$, with the average vector between them denoted as $\boldsymbol{e}_1^m$ (located in the middle corner of Figure 2). Unlike [11], in this study, we do not

use the vector $\boldsymbol{e}_3$ to calculate the rotation vector $\boldsymbol{\alpha}_\Delta$. Instead, we employ the vector $\boldsymbol{e}_1$, which can be computed solely using the displacement field. After defining $\boldsymbol{\alpha}_\Delta$ (solely based on displacements and φ_Δ), we can determine $\boldsymbol{Q}_\Delta$, which is applied in the shell kinematics (rotating the shell director $\boldsymbol{e}_3$, as discussed previously).

Through algebraic manipulation of previous Equations, and considering more detailed explanation in [1], it can be demonstrated that

$$\boldsymbol{e}_1^{i+1} - \boldsymbol{e}_1^{i} = \boldsymbol{\alpha}_\Delta \times \boldsymbol{e}_1^{m} \quad \text{where} \quad \boldsymbol{e}_1^{m} = \frac{1}{2}\left(\boldsymbol{e}_1^{i+1} + \boldsymbol{e}_1^{i}\right) \quad \text{and} \quad \boldsymbol{\alpha}_\Delta = \frac{\boldsymbol{e}_1^{i} \times \boldsymbol{e}_1^{i+1}}{\|\boldsymbol{e}_1^{m}\|^2} + \varphi_\Delta \frac{\boldsymbol{e}_1^{m}}{\|\boldsymbol{e}_1^{m}\|} \quad . \tag{15}$$

2.3 Variational formulation, Strain Energy, Neo-Hookean material

The Neo-Hookean isotropic material discussed in this section, which forms the basis for most of the numerical examples in this paper, is defined by the polyconvex strain energy function as follows. Other material formulation may be checked in [1]:

$$\psi = \frac{1}{2}\lambda\left(\frac{1}{2}\left(J^2 - 1\right) - \ln\left(J\right)\right) + \frac{1}{2}\mu\left(I_1 - 3 - 2\ln\left(J\right)\right) \qquad \text{where:} \tag{16}$$

- $I_1 = \text{tr}, \boldsymbol{C} = \boldsymbol{f}_i \cdot \boldsymbol{f}_i$
- $I_2 = \text{tr}\left[\text{Cof}\ \boldsymbol{C}\right] = \boldsymbol{g}_i \cdot \boldsymbol{g}_i$
- $I_3 = \det \boldsymbol{C} = J^2 = \left(\boldsymbol{f}_1 \cdot \left(\boldsymbol{f}_2 \times \boldsymbol{f}_3\right)\right)^2$
- λ and μ - Lamé coefficients (representing material properties)
- $\psi = \psi\left(\boldsymbol{F}\right)$ - Helmholtz free energy (Strain energy function)
- $\boldsymbol{C} = \boldsymbol{F}^T\boldsymbol{F}$ - Right Cauchy-Green tensor.

3 Finite Element

This article presents a triangular element configuration featuring 6 nodes. Within this setup, displacements are described by a quadratic interpolated field, while an additional scalar rotation parameter is incorporated into each of the central-side nodes. By combining this scalar with the displacement Degrees of Freedom (DoF), it is possible to formulate a non-conformal, incremental, linear rotational field. For a more comprehensive understanding, please refer to [1].

The central-side node, situated precisely midway between the corner-nodes, plays a pivotal role in this context. Furthermore, it's important to mention that the element begins in a flat state, without any curvature. This characteristic ensures that membrane locking, as discussed in [10], is not anticipated.

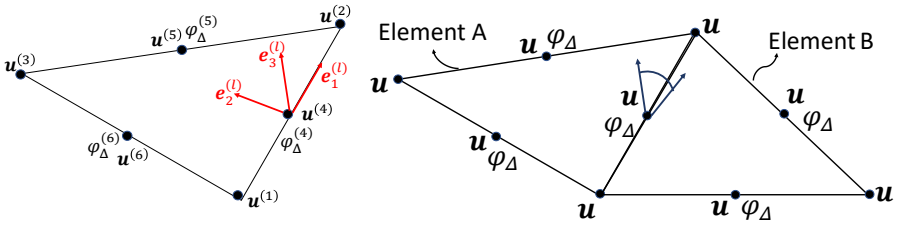

Figure 3. 6-Node Shell element DOF.

The rotation vector $\boldsymbol{\alpha}$ is an internal-calculated variable of the shell finite element and is defined within a nonconforming linear field structure similar to the approach presented in [5]. However, in contrast to having $\boldsymbol{\alpha}$ as a nodal degree of freedom (DOF), we derive it using the displacements and a scalar parameter φ_Δ. This scalar φ_Δ is the actual DOF that is shared between neighboring elements. This novel approach constitutes a significant advancement in this model and support several key kinematic aspects of this formulation. The rotation field is no longer an entirely independent field that is decoupled from displacement. Instead, rotation is now constructed in conjunction with displacement and a rotation-related scalar DOF.

From previous equations, the displacement-dependent aspect of $\boldsymbol{\alpha}_\Delta$ is determined using $\boldsymbol{e}_1^{i}$ and $\boldsymbol{e}_1^{i+1}$. Utilizing Equation 7, it can be verified that the normalized tangent vector at the midside nodes for both time steps t^i and t^{i+1} is computed as:

$$\boldsymbol{e}_1 = \frac{\boldsymbol{z}_{,1}}{\|\boldsymbol{z}_{,1}\|} \quad \text{with} \quad \boldsymbol{z}_{,1} = \boldsymbol{e}_1^r + \boldsymbol{u}_{,1} \ . \tag{17}$$

Concerning the equations above, it is noteworthy that in the triangular element with six nodes (characterized by a quadratic displacement field), the derivative $u_{,1}$ is solely a function of the vertex displacement. The node numbering scheme is presented in Figure 3, and these nodes are employed in defining $\boldsymbol{u}_{,1}$ (see [1].

From previous equations, it can be seen that the rotational field computed at the element's sides is determined by the degrees of freedom shared among neighboring elements. Consequently, even though $\boldsymbol{\alpha}$ is internally computed within each element, it remains numerically consistent across all simulation steps for adjacent elements. This consistency in the rotation maintains the continuity of the rotational field at midside nodes, a foundational attribute of this shell kinematic model. It's important to note that enforcing rotation continuity only at the midside nodes does not pose a problem (as discussed in [5] and [4]).

Another important feature in this element, is that the rotation is introduced incrementally. Consequently, during each step increment, the rotation vector $\boldsymbol{\alpha}$ is updated and is utilized in accordance with Equations 14 and 15.

Since an incremental approach is utilized to evaluate the rotation field and curvature, the incremental parameters must be reset at every load step. For each load step, the element recalculates these incremental parameters to determine the final values for these fields. Consequently, at each load step at the finite element level we must enforce $\boldsymbol{\alpha}_\Delta = 0$, $\varphi_\Delta = 0$.

4 Numerical examples

This section presents numerical examples assessing the element's reliability under various loading and stress conditions. A more complete set of examples and test und different conditions is presented in [1]. Due to consiseness in this article, we are going to present only 3 important examples, in order to demonstrate: 1) numerical stability; 2) locking behavior; 3) large displacements and rotations.

Simulated outputs are compared with literature data, acknowledging potential differences due to distinct shell element assumptions. Such small variations in displacement may arise from model differences like shear-rigid, shear-flexible, and rod models.

4.1 Square plate—linear bending locking analysis

In this examples, we employ the shell element to replicate the behavior of a square plate with simple supported sides, subjected to a uniformly distributed vertical load (q) within the linear range. This scenario aligns with simulations conducted in [5] and [13], specifically targeting the analysis of bending-locking effects. The plate possesses a planar structure, and when dealing with slender thickness, the utilization of shell elements leads to a phenomenon known as locking, where the elements exhibit unrealistic stiffness, resulting in nearly negligible displacements. Since only the initial simulation step is executed, the stiffness matrix lacks the inclusion of membrane effects.

The geometry is presented in Figure 4 together with the graph of normalized vertical displacement. Key attributes of the plate include a side length (L) of 2000, material constants (E and ν) set at 1000 and 0.3 respectively, and thickness (h) ranging across values of 0.2, 0.02, 0.002, 0.0002, 0.00002, and 0.000002. The reference point for vertical displacement adheres to the classical analytical Kirchhoff solution expressed as $w_{Kirchhoff} = 0.0444qL^4/Eh^3$ ([14] and [15]) for a square plate under simple support conditions. The results demonstrate convergence of the element, particularly evident for extremely thin plates until the ratio h/L reaches 1×10^{-6}.

4.2 Pinched cylinder

This example has been a recurring topic in shell studies, extensively discussed across various articles (refer to [5], [16], [4], [17], [13], [2]). The cylinder possesses a radius (R) of 100, length (L) of 200, and thickness (h) of 1. The shell's mechanical properties are characterized by $E = 30 \cdot 10^3$ and $\nu = 0.3$, while the applied pinching force is denoted as $P = 20000$.

The depiction of the cylinder FEM model can be observed in Figure 5, also with the vertical displacement of point A and horizontal displacement of point B vs applied force. These displacements are

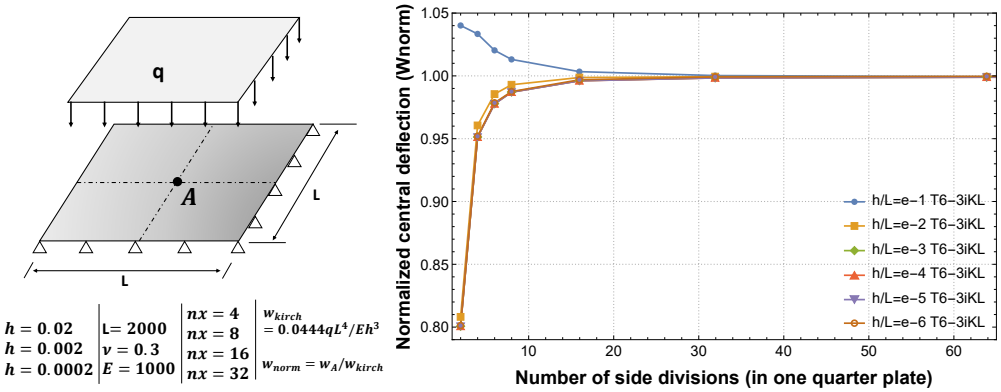

Figure 4. Square Plate - Linear bending locking analysis. Normalized Central Deflection vs Side division in on quarter plate

compared using both a coarse mesh (6272 elements with 28 side elements per one-quarter of the cylindrical shell) and a fine mesh (10368 elements with 36 side elements per one-quarter of the cylindrical shell). The simulation results exhibit a close alignment with the findings in existing literature, specifically the works of Viebahn [4] and Sze [17].

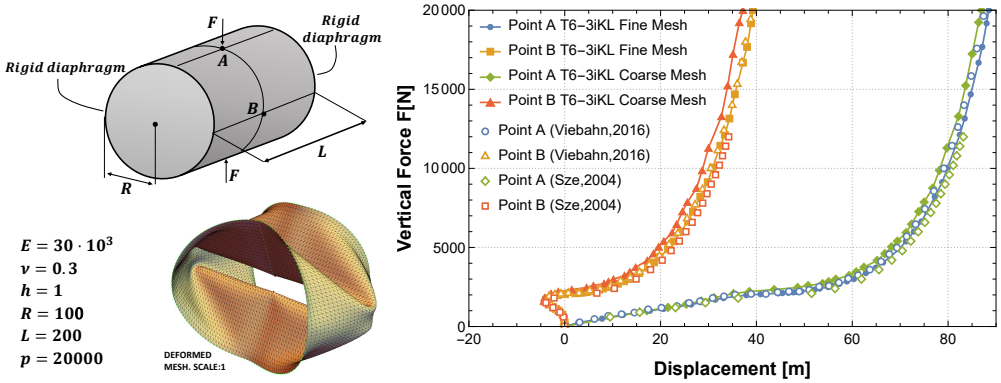

Figure 5. Pinched cylindrical shell mounted on rigid end diaphragms. Vertical force vs vertical (Point A) and lateral (Point B) displacement.

5 Conclusions

This paper introduces a triangular nonlinear finite element suitable for large displacement, strains and rotations of thin and very thin shells. It's simple and has demonstrated to be reliable. It uses a quadratic displacement field, a linear rotation fild built from displacements and a scalar rotation DoF. No extra numerical parameters such as penalty methods, or Lagrange multipliers are required. This new element does not present shear locking like other elements available in literature.

Numerical examples in section 4 highlight the method's prowess, reliability in linear/non-linear scenarios: elastic stability, buckling, bending, varied stresses, shell-locking, multibranched shells, thickness changes, anisotropic membranes (see more into [1]).

Acknowledgements. Matheus, Paulo and Adnan extend their gratitude for the support provided by ANR-FAPESP through the thematic grant 2020/13362-1, titled "Mechanics, Stochastics and Control with Code-Coupling: System-of-Multibody-Systems point-of-view to Optimize Off-Shore/In-Land Farms of Wind Turbines with Flexible Blades" (MS3C project), which enabled the realization of this work. Matheus Lucci Sanchez expresses his appreciation to Clark Solutions, his employer, where he works as a project engineer, for their financial backing, knowledge sharing, practicality, and industrial expertise. P. M. Pimenta acknowledges the support from CNPq under grant 308142/2018-7 and the Alexander von Humboldt Foundation for the Georg Forster Award, which facilitated his stays at the Universities of Duisburg-Essen and Hannover in Germany.

Authorship statement. The authors hereby confirm that they are the sole liable persons responsible for the authorship of this work, and that all material that has been herein included as part of the present paper is either the property (and authorship) of the authors, or has the permission of the owners to be included here.

References

[1] M. L. Sanchez, P. M. Pimenta, and A. Ibrahimbegovic. A simple geometrically exact finite element for thin shells—part 1: statics. *Computational Mechanics*, pp. 1–21, 2023.
[2] M. L. Sanchez, P. M. Pimenta, and Costa e C. Silva. A simple fully nonlinear Kirchhoff-Love shell finite element. *Latin American Journal of Solids and Structures*, vol. 17, n. 8, 2020.
[3] Costa e C. Silva, S. F. Maassen, P. M. Pimenta, and J. Schröder. On the simultaneous use of simple geometrically exact shear-rigid rod and shell finite elements. *Computational Mechanics*, vol. 67, n. 3, pp. 867–881, 2021.
[4] N. Viebahn, P. M. Pimenta, and J. Schröder. A simple triangular finite element for nonlinear thin shells: statics, dynamics and anisotropy. *cm*, vol. 59, n. 2, pp. 281–297, 2017.
[5] E. M. B. Campello, P. M. Pimenta, and P. Wriggers. A triangular finite shell element based on a fully nonlinear shell formulation. *Computational mechanics*, vol. 31, n. 6, pp. 505–518, 2003.
[6] J. Argyris. An excursion into large rotations. *Computer methods in applied mechanics and engineering*, vol. 32, n. 1-3, pp. 85–155, 1982.
[7] P. M. Pimenta and E. M. B. Campello. Geometrically nonlinear analysis of thin-walled space frames. In *Proceedings of the second european conference on computational mechanics, II ECCM, Cracow, Poland*, 2001.
[8] P. M. Pimenta, E. M. B. Campello, and P. Wriggers. An exact conserving algorithm for nonlinear dynamics with rotational dofs and general hyperelasticity. part 1: Rods. *Computational Mechanics*, vol. 42, n. 5, pp. 715–732, 2008.
[9] E. M. B. Campello, P. M. Pimenta, and P. Wriggers. An exact conserving algorithm for nonlinear dynamics with rotational dofs and general hyperelasticity. part 2: shells. *Computational Mechanics*, vol. 48, n. 2, pp. 195–211, 2011.
[10] P. M. Pimenta and E. M. B. Campello. Shell curvature as an initial deformation: a geometrically exact finite element approach. *International journal for numerical methods in engineering*, vol. 78, n. 9, pp. 1094–1112, 2009.
[11] Costa e C. Silva, S. F. Maassen, P. M. Pimenta, and J. Schröder. A simple finite element for the geometrically exact analysis of Bernoulli-Euler rods. *Computational Mechanics*, pp. 1–19, 2019.
[12] Costa e C. Silva. *Geometrically exact shear-rigid shell and rod models.* PhD thesis, Polytechnic School at University of São Paulo, 2020.
[13] Y. Ko, Y. Lee, P. S. Lee, and K. J. Bathe. Performance of the mitc3+ and mitc4+ shell elements in widely-used benchmark problems. *Computers & Structures*, vol. 193, pp. 187–206, 2017.
[14] W. C. Young, R. G. Budynas, and A. M. Sadegh. *Roark's formulas for stress and strain.* McGraw-Hill Education, 2012.
[15] S. Timoshenko, S. Woinowsky-Krieger, and others. *Theory of plates and shells*, volume 2. McGraw-hill New York, 1959.
[16] P. M. Pimenta, E. M. B. Campello, and P. Wriggers. A fully nonlinear multi-parameter shell model with thickness variation and a triangular shell finite element. *Computational Mechanics*, vol. 34, n. 3, pp. 181–193, 2004.
[17] K. Y. Sze, X. H. Liu, and S. H. Lo. Popular benchmark problems for geometric nonlinear analysis of shells. *Finite elements in analysis and design*, vol. 40, n. 11, pp. 1551–1569, 2004.